

Research Paper

Ultrasonic Experimental Evaluation of the Numerical Model of the Internal Fluid Flow in the Kidney Cooling Jacket

Barbara GAMBIN^{(1)*}, Ilona KORCZAK-CEGIELSKA⁽²⁾, Wojciech SECOMSKI⁽¹⁾,
Eleonora KRUGLENKO⁽¹⁾, Andrzej NOWICKI⁽¹⁾

⁽¹⁾ *Department of Ultrasound
Institute of Fundamental Technological Research, Polish Academy of Sciences
Warsaw, Poland*

⁽²⁾ *Doctoral Studies of Institute of Fundamental Technological Research, Polish Academy of Sciences
Warsaw, Poland*

*Corresponding Author e-mail: bgambin@ippt.pan.pl

(received January 11, 2022; accepted May 4, 2022)

Kidney Cooling Jacket (KCJ) preserves the kidney graft, wrapped in the jacket, against the too fast time of temperature rise during the operation of connecting a cooled transplant to the patient's bloodstream. The efficiency of KCJ depends on the stationarity of the fluid flow and its spatial uniformity. In this paper, the fluid velocity field inside the three different KCJ prototypes has been measured using the 20 MHz ultrasonic Doppler flowmeter. The simplified 2D geometrical model of the prototypes has been presented using COMSOL-Multiphysics to simulate the fluid flow assuming the laminar flow model. By comparing the numerical results with experimental data, the simplified 2D model is shown to be accurate enough to predict the flow distribution of the internal fluid velocity field within the KCJ. The discrepancy between the average velocity measured using the 20 MHz Doppler and numerical results was mainly related to the sensitivity of the velocity measurements to a change of the direction of the local fluid flow stream. Flux direction and average velocity were additionally confirmed by using commercial colour Doppler imaging scanner. The current approach showed nearly 90% agreement of the experimental results and numerical simulations. It was important for justifying the use of numerical modelling in designing the baffles distribution (internal walls in the flow space) for obtaining the most spatially uniform field of flow velocity.

Keywords: multi-canal system; fluid flow prediction; cooling jacket; flow Doppler measurement.



Copyright © 2022 B. Gambin *et al.*
This is an open-access article distributed under the terms of the Creative Commons Attribution-ShareAlike 4.0 International (CC BY-SA 4.0) <https://creativecommons.org/licenses/by-sa/4.0/> which permits use, distribution, and reproduction in any medium, provided that the article is properly cited, the use is non-commercial, and no modifications or adaptations are made.

1. Introduction

The organ intended for transplantation, after being removed from the donor, is stored at low temperature unless it is connected to a device supporting its vital functions. The temperature of 4°C sufficiently reduces the metabolism rate of cells to maintain their ability of taking up life functions under more favourable conditions. The cells and the organs including kidneys can be preserved outside the body at the temperature of 4°C before the transplantation to avoid the negative effects of a “warm ischemia” (MOERS *et al.*, 2012). The temperature of the organ removed from the container with a temperature of 4°C must not rise too rapidly

during the transplantation surgery until the blood supply is connected. This would risk having the negative effects of the “second warm ischemia”. The surface of the organ adjacent to the tissues of the body cavity at a temperature of about 36–37°C during the transplantation may be permanently damaged due to rapid heating, which leads to complications and may result in rejection of the transplant. However, optimal solutions such as living donor transplantation are still not common. It is also not popular practice to support extracorporeal organ life by artificial blood circulation until transplantation because of the additional high costs of special equipment. Most transplants require appropriate procedures after organ removal until their

work starts after transplantation surgery. Recently, the necessity of intracorporeal cooling of graft during the implantation procedure (HEYLEN *et al.*, 2021; KHAN *et al.*, 2021) was strongly underlined. In the latter, a cooling jacket made from two kinds of isolation films is described. The preliminary experiments *ex vivo* performed in a water bath showed the device's usefulness against heat transport from the external environment to the cooled organ during one hour. In this paper, we studied an internal cooling flow in the new device, patented recently by the second author of the paper (KORCZAK-CEGIELSKA *et al.*, 2022). It has the form of a jacket, named Kidney Cooling Jacket (KCJ), in which an organ can be placed during the procedure. The shape of the pocket provides access for the surgeon to the part of the kidney with the vessels connecting the organ with the blood circulation. The usefulness of the patent has been already confirmed in (BREDA *et al.*, 2022) *in vivo* experiments. The cooling flow system of the KCJ was designed taking into account the cost, ease of production, quality of materials, reliability, and the internal flow uniformity. The KCJ equipped with an active flow cooling system should eliminate or at least shorten the second warm ischemia time. The internal fluid flow in the KCJ should be stationary and spatially homogeneous. In particular, areas of stagnation called “flow dead zones”, where ambient heat will dominate over the cooling by the flowing fluid and will cause unfavourable heating of the kidney placed inside the KCJ, should be eliminated. The elimination of dead areas is related to the design of the shape of the jacket, more precisely, its geometric structure in the form of internal partitions positioning influencing the flow characteristics. The designing process cannot be performed without the numerical modelling of the flow inside the complicated flow space in the KCJ. The paper aims to construct and experimentally validate the numerical model of KCJ internal flow useful in the design of the KCJ form to ensure the uniformity and stationarity of the cooling flow. To this end, we built the simplified 2D numerical model of the liquid flow inside the complicated system of KCJ channels of the fabricated KCJ prototype. We use the model in the further predictions of the temperature distribution due to the heat transport by convection coupled with the internal flow circulating inside the KCJ walls. In the paper, we demonstrate an ultrasonic evaluation of the flow velocity spatial distributions obtained from the numerical model. To this end, we compare the flow velocity field measurements made by the custom designed in Institute of Fundamental Technological Research Polish Academy of Sciences (IPPT PAN) vascular 20 MHz Doppler flowmeter (SECOMSKI *et al.*, 2009) with the numerical model predictions. The 20 MHz Doppler measurements were also validated by the colour Doppler imaging (Ultrasonix, Ultrasonix Sonix Touch-Research, Ultrasonix Medical Corpora-

tion, Richmond, BC, Canada). We will discuss the relative errors between the ultrasonic experimental results, i.e. the internal flow velocity spatial distribution in the KCJ walls, to the numerical values of the flow field obtained from the modelling. We discuss here the physical background of the different errors related to the flow characteristics and the limitation of the 2D modelling.

2. Materials and methods

2.1. Kidney Cooling Jacket and the flow inside its side walls characteristics

The Kidney Cooling Jacket is in the form of a bag in which an organ can be inserted during transplantation, see Fig. 1.

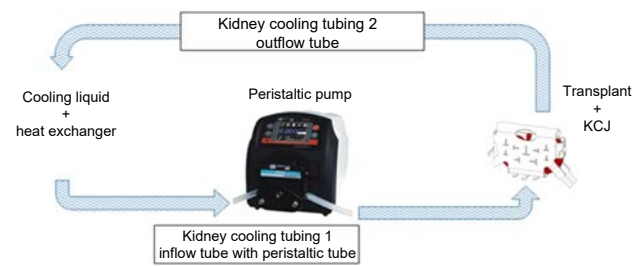


Fig. 1. Scheme of the KCJ.

The side walls forming the KCJ are double, made of a thin biocompatible polymer film. Cooling fluid circulates between the walls. The fluid flow is forced by gravity or controlled by a suitably designed peristaltic pump. Since KCJ is supposed to keep the temperature of the kidney organ low during the transplantation procedure, more precisely, in the temperature range of 4–15°C during one hour, the aim was to design a flow space to provide uniformly cooling surfaces of the KCJ having a direct contact to the organ inserted into the KCJ.

The geometry of the flow space model proposed below is a 2D geometry, the space limited by the external wall surfaces and internal walls (in the form of a letter T), which is the direct image of the 2D project of 3 produced prototypes of 3 sizes: S (small), M (medium), L (large). In Fig. 2 the geometry of the projections of the “cut” KCJ on the plane is depicted together with the technical dimensions used in the numerical model.

In Fig. 3c there are two photos of the two KCJ outer surfaces.

Assuming that the fluid circulates in 2D space is a strong simplification. In reality, the fluid circulates between KCJ walls in an irregular three-dimensional space delimited by two KCJ wall shells and T-shaped welds of the walls creating together a complicated system of flow canals. The arrangement of the welds ensures a spatially uniform flow, breaking the inlet main liquid stream into many smaller streams. The arrange-

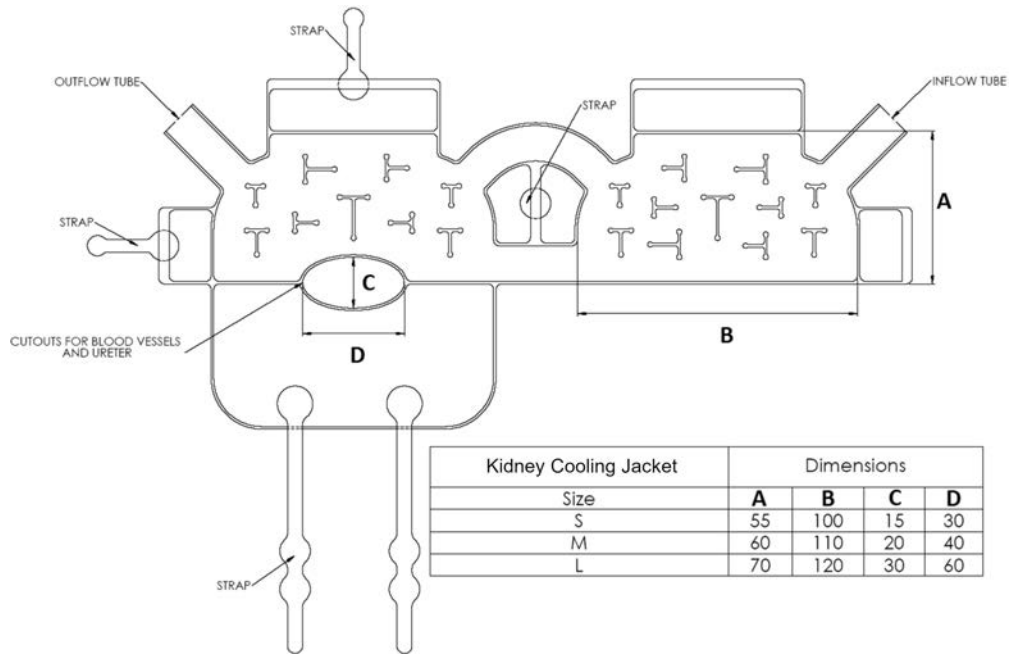


Fig. 2. Technical sizes of the prototypes KCJ device: S (small), M (medium), L (large). The numbers in the inserted table are given in [mm].

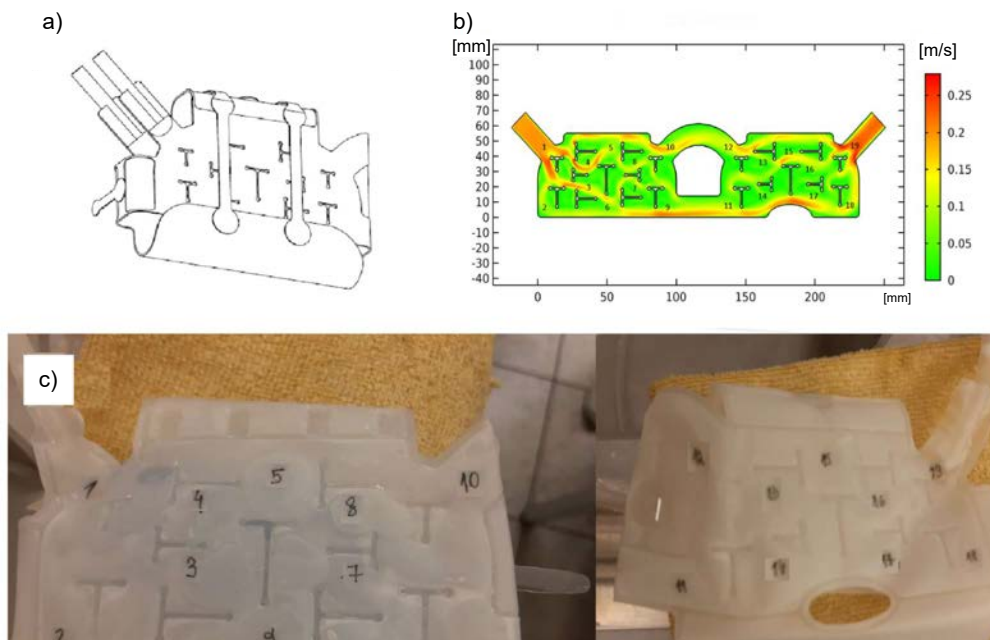


Fig. 3. Kidney Cooling Jacket and Doppler measurement points: a) 3D scheme of KCJ; b) the numbering of measurement points on the background of the numerical prediction of flow velocities; c) the measurement points marked on the prototype S of Kidney Cooling.

ment of molds in the prototypes was designed based on performing many numerical calculations and choosing the optimal model with the most uniform flow velocity field inside the flow space. The experimental validation of the numerical model was performed by using the ultrasonic Doppler measurements of flow field velocities. It should be stressed that assumptions on the flow character in such a complex flow system are important

for modelling. The length diameter D , characterising the flow under consideration, is variable at different points of the KCJ. The length diameter D characterising the flow under consideration, is variable at different points of the KCJ. The maximum D value is 12 mm for the prototype of size S.

The wall thickness, the third dimension of the flow, after filling the KCJ with liquid is less than 10 mm.

The fluid has been specially prepared to be filled with starch imitating fine particles acting as ultrasound scatters. The viscosity of starch-admixed water was in the order of $1.0034 \text{ mm}^2/\text{s}$ at room temperature. The Reynolds number (Re), characterising the flow character is expressed by the formula:

$$\text{Re} = \frac{\rho \cdot u \cdot D}{\nu}, \quad (1)$$

where ρ is the density of the fluid, u flow speed, D is a characteristic linear dimension, and ν is the dynamic viscosity of the fluid. This means that the flow is characterised by the Reynolds number lower than 2100 if the flow velocity does not exceed 211 mm/s and can be modelled as laminar flow assuming that the characteristic flow space dimension is equal to 10 mm , i.e. equal to the maximum size of inter-wall distance inside the KCJ of the S size.

Note that the fluid circulating in the KCJ has a temperature lowered down to 4°C while the operation is in progress. Then the laminar flow is ensured up to the speed of 300 mm/s , because of the increased kinematic viscosity to the value of $1.5674 \text{ mm}^2/\text{s}$. The curvature of the local canal in which the flow takes place also influences the flow laminarity. The dimensionless quantity characterising the flow in curved channels is the Dean number (De) which is expressed by the following formula:

$$\text{De} = \text{Re} \sqrt{\frac{D}{2R_c}}, \quad (2)$$

where D is the diameter (for non-circular geometry, an equivalent diameter is used), R_c is the radius of curvature of the path of the canal, and Re is the Reynolds number.

The Dean number is therefore the product of the Reynolds number (based on axial flow v through a canal of diameter D) and the square root of the ratio between characteristic geometrical parameter and the curvature “diameter”, i.e. $2 \cdot R_c$. For $\text{De} \leq 40\text{--}60$ the flow can be considered as completely unidirectional. As the Dean number increases from the range of $40\text{--}60$ to the range of $64\text{--}75$, some wavy perturbations can be observed in the cross-section, and the fully turbulent flow forms for $\text{De} \geq 400$.

2.2. FEM model of the internal flow inside KCJ side walls coupled with convective heat transport

The mathematical model consists of basic equations of flow in KCJ walls and is coupled with the flow heat transfer equation. We assume that the flow inside the jacket is laminar, stationary, and the fluid is incompressible, then the Navier-Stokes equations for flow velocity \mathbf{u} read as follows:

$$\begin{aligned} \rho(\mathbf{u} \cdot \nabla)\mathbf{u} &= \nabla \cdot [-2p\mathbf{I} + \mathbf{K}] + \mathbf{F}, \\ \rho \nabla \cdot \mathbf{u} &= 0, \end{aligned} \quad (3)$$

where the stress tensor \mathbf{K} is equal to $\mathbf{K} = \mu(\nabla\mathbf{u} + (\nabla\mathbf{u})^T)$, ρ denotes fluid density, p is the fluid pressure, μ is the fluid viscosity, ∇ is the gradient vector, \cdot denotes the simple tensor contraction, \mathbf{F} is the body forces, and symbol T in upper index denotes tensor transposition, respectively.

To simplify the calculations we assume that the fluid properties are constant in the considered range of temperature ($4\text{--}15^\circ\text{C}$). So, the coupling of temperature and fluid flow is here “one-sided”, the temperature changes do not influence the material properties. The temperature distribution inside the KCJ is caused by the flow and is calculated from the following equation of convective heat transfer:

$$\rho C_p \mathbf{u} \cdot \nabla T + \nabla \cdot \mathbf{q} = Q, \quad (4)$$

with the Fourier law for heat flux \mathbf{q} written as $\mathbf{q} = \kappa \nabla T$, where C_p denotes specific heat, T is the temperature, Q denotes the body heat sources, and κ stands for the fluid heat conductivity, respectively.

The 2D geometry of the flow space inside the KCJ walls together with the scheme of the boundary conditions imposed to Eqs (3) and (4) is depicted in Fig. 4.

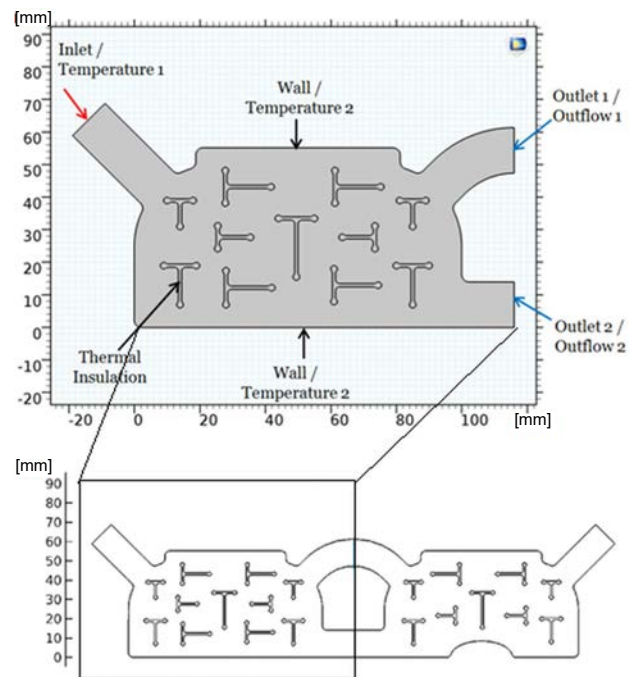


Fig. 4. Geometry of the flow space and the scheme of the imposed boundary conditions.

We performed FEM calculations using COMSOL Multiphysics 4.3b software and the Module of Heat Transfer in Fluid. For the considered problem, a mesh consisting of triangular and quadrilateral elements was defined. The total number of triangular elements was 8342, the number of quadrilateral elements was 1672.

2.3. Ultrasonic Doppler measurements

Flow rates were measured with an ultrasonic pulse-Doppler flow meter. The Doppler effect causes the acoustic wave scattered on the moving particles in the suspension to have a different frequency than the transmitted wave. The ultrasonic wave backscattered on the moving particles is shifted in the frequency by the so called Doppler frequency equal to $f_d = 2f_n \frac{v}{c} \cos \theta$, where f_d denotes Doppler frequency, f_n is the frequency of the transmitted wave, v is the speed of moving particles, c stands for the wave velocity in the medium, θ denotes the angle between the direction of the flow and the direction of incidence of the ultrasonic wave, respectively. As the particles move at different velocities, the Doppler signal has a frequency spectrum that corresponds to the quantitative velocity distribution of the suspended particles.

An ultrasonic (transmitting/receiving) transducer was placed above the flowing liquid. The received signal was recorded in the spatially positioned receiving sample volume, SV, called Doppler gate. The SV has the shape of a cylinder, the diameter of which corresponds to the width of the ultrasonic beam and the thickness to the time duration of the gate in the flow meter receiver. The relationship between the gate depth Δz and the delay Δt , being the time between the start of the transmit pulse and the gate turn-on time, is given by the formula: $\Delta z = 1/2\Delta t \cdot c$.

The small changes in the angle θ result in a significant difference in the final measurement of the Doppler frequency, i.e. with the determination of the local velocity of the liquid flow. Hence, for precise velocity measurement a precise definition of the angle θ is crucial. That means that it is important to control the direction of flow concerning the direction of the ultrasound beam axis. Assuming the angle $\theta = 60^\circ$ the error in the real positioning of the transducer equal to of $\pm 5^\circ$

results in the $\pm 15\%$ error of the velocity estimation. Errors in angles greater than 20° may result in erroneous estimation of flow velocity exceeding 100%. The fluid velocity measurements were performed with the use of the Doppler pulse meter working at the ultrasonic frequency of 20 MHz, developed at the Department of Ultrasound IPPT PAN, marked in the experimental setup in Fig. 5.

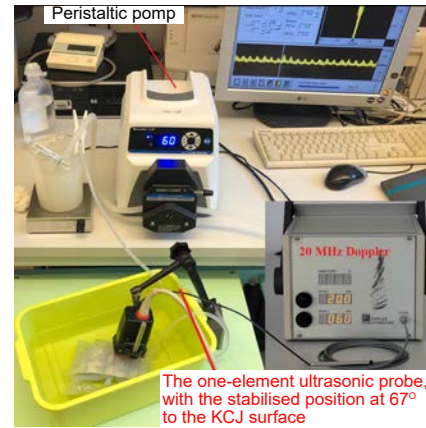


Fig. 5. Scheme of the experimental setup for measuring the velocity field inside the KCJ.

The flowmeter was connected to the acquisition board – FFT Multigate Doppler developed by Tortoli group in Florence (BAMBI *et al.*, 2004). The dedicated software allows for recording and analysis of the Doppler spectra in 128 consecutive gates distant at 0.075 mm covering the penetration depth of 9.6 mm.

The software enables both the registration of the flow velocity profile and the determination of the average velocity, averaged over both the time and depth. The recorded flow profile and the instantaneous frequency spectrum of the Doppler signal as a function of time are shown in Fig. 6. The Doppler frequency

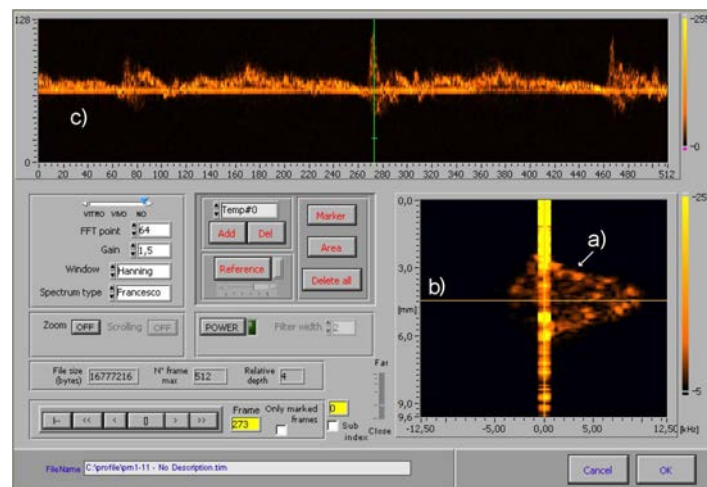


Fig. 6. Recorded Doppler spectra in 128 gates: a) instantaneous flow profile constructed from 128 FFT spectra of a Doppler signal; b) position of the gate (4.5 mm) from which the spectrum is displayed in box c); c) frequency spectrum of the Doppler signal as a function of time.

spectrum is recorded from the Doppler gate located 4.5 mm under the Jacket surface.

3. Results and discussion

The FEM model enables the analysis of both the velocity field of a fluid in a 2D flow system and the pressure field. A constant velocity was set on the inflow, equal to the average velocity obtained at this point from the Doppler measurement. The liquid outflow was free. Figure 7 shows a finite element mesh, the calculated flow velocities, and the temperature field distribution.

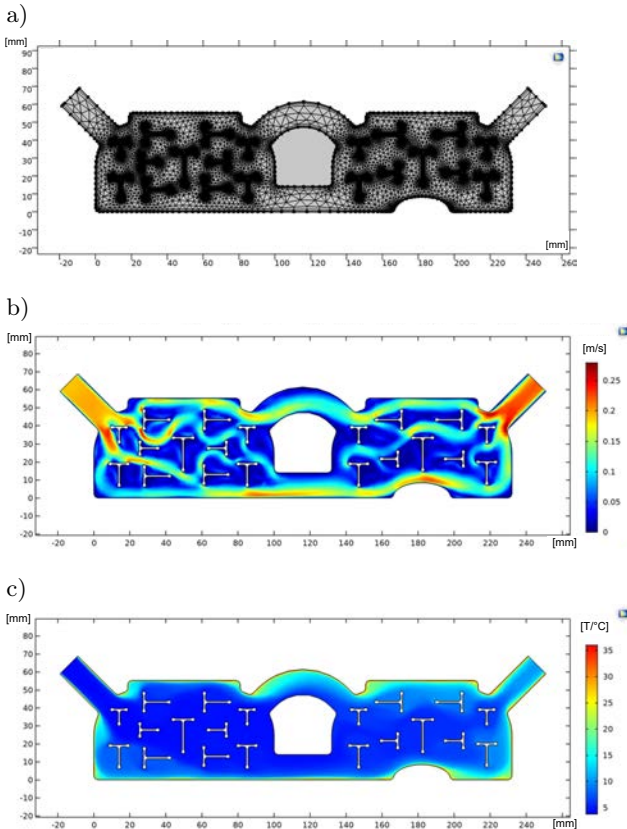


Fig. 7. FEM calculations: a) mesh; b) velocity field; c) temperature field.

In rectilinear flow sections, the mesh is rather rare but significantly denser around T-shaped internal wall partitions. Assuming that the entering liquid has a temperature of around 5°C and the edge has a temperature of 37°C, the temperature distribution is almost homogeneous. A temperature less than 7°C has 90% of the area. Figure 8 shows the flow pressure drop from the inlet to the outlet.

The uniform nature of the pressure gradient confirmed the effective breakdown of the liquid stream through the baffles so that the flow is consequently spatially uniform. The maps of the horizontal and vertical components of the flow velocity direction compared with the velocity values shown in Fig. 9 confirm

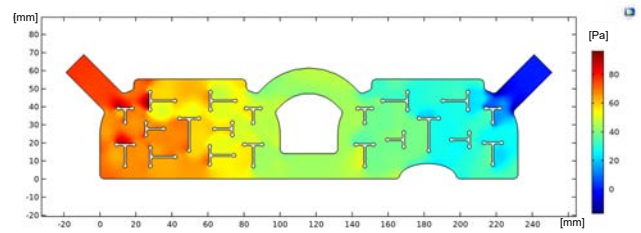


Fig. 8. Pressure field distribution.

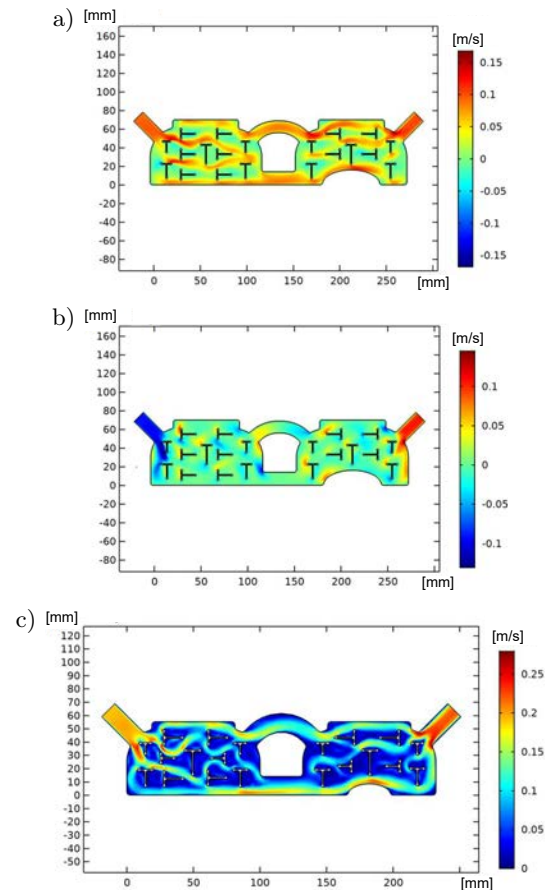


Fig. 9. Velocity field: a) x -components; b) y -components; c) magnitude.

that c/a 80% of the area is dominated by movement in the x -axis direction. The obtained results illustrate the curvature of the main streams of the fluid flow.

These streams bypass the baffles and the shape of the flow path has much less curvature than the curvature of the edges of the baffles. 10 velocity profiles were traced across the stream direction near each of the 19 measurement points. They were used to determine the average velocity around the points. The use of a multi-gate Doppler allowed to increase the accuracy of the flow velocity measurements compared to Doppler velocity measurements by Ultrasonix apparatus. The power of the signal scattered on the particles of the suspension is proportional to the fourth power of the frequency. With an increase in the ultrasonic frequency from 6.6 MHz (in the Ultrasonix apparatus)

to 20 MHz (in the used by us multi-gate Doppler), the power of the Doppler signal increases several dozen times (or almost 20 dB). This increases the signal-to-noise ratio by a similar amount. The second factor increasing the accuracy was the multi-gate measurement taking into account the actual fluid flow profile. The example of mean velocity flow profile estimation in the measurement point no. 1 is shown in Fig. 10. The ‘‘Doppler beam’’ was set to cross the colour flow map at the angle of 60°. Coolant flow velocity measurements were verified by using the colour Doppler imaging technique (EVANS *et al.*, 2011). The L14-5/38 linear transducer operating at the frequency of 10 MHz for imaging and at 6.6 MHz for colour and Doppler spectrum Doppler recording was used.

The high compliance of the shape of calculated profiles to those measured by Doppler should be emphasized.

Figure 11 shows the sections near point no. 3 with five calculated profiles and two profiles obtained from the Doppler measurement.

The average velocities for all 19 points, whose positions are shown in Figs 3a and 3b, numerically calculated and measured by Doppler are given in Table 1.

If we consider a stationary fluid flow in a pipe with a circular cross-section, the velocity distribution in each plane passing through the direction parallel to the pipe axis is the same. The numerically obtained 2D velocity distribution was calculated in a plane parallel to the walls of KCJ, whereas the Doppler measurement was performed in a plane locally per-

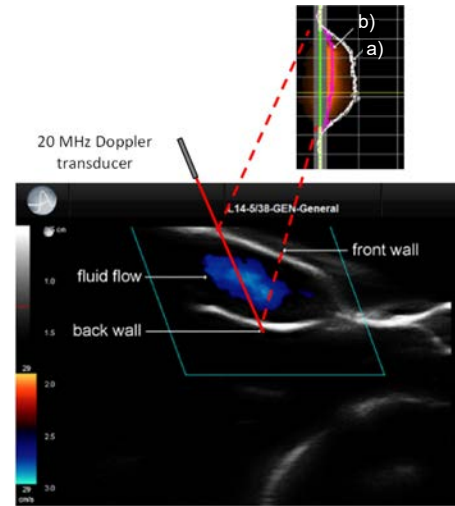


Fig. 10. Ultrasonic B-mode image and Doppler colour flow map of the Kidney Cooling Jacket. The red line denotes the Doppler signal direction, the angle between flow direction and Doppler beam equals to 60°: a) the peak velocity flow profile constructed from 128 FFT spectra of the Doppler signal; b) mean velocity flow profile averaged over time and frequency. Mean velocity averaged across the vessel = 0.16 m/s.

pendicular to the side walls. So, the agreement of the Doppler measurement with the results of the numerical calculations is as accurate as the replacement of the local flow inside the KCJ walls by the flow in the circular pipe. In the reality, the walls of the KCJ are corrugated and the flow takes place in between curving,

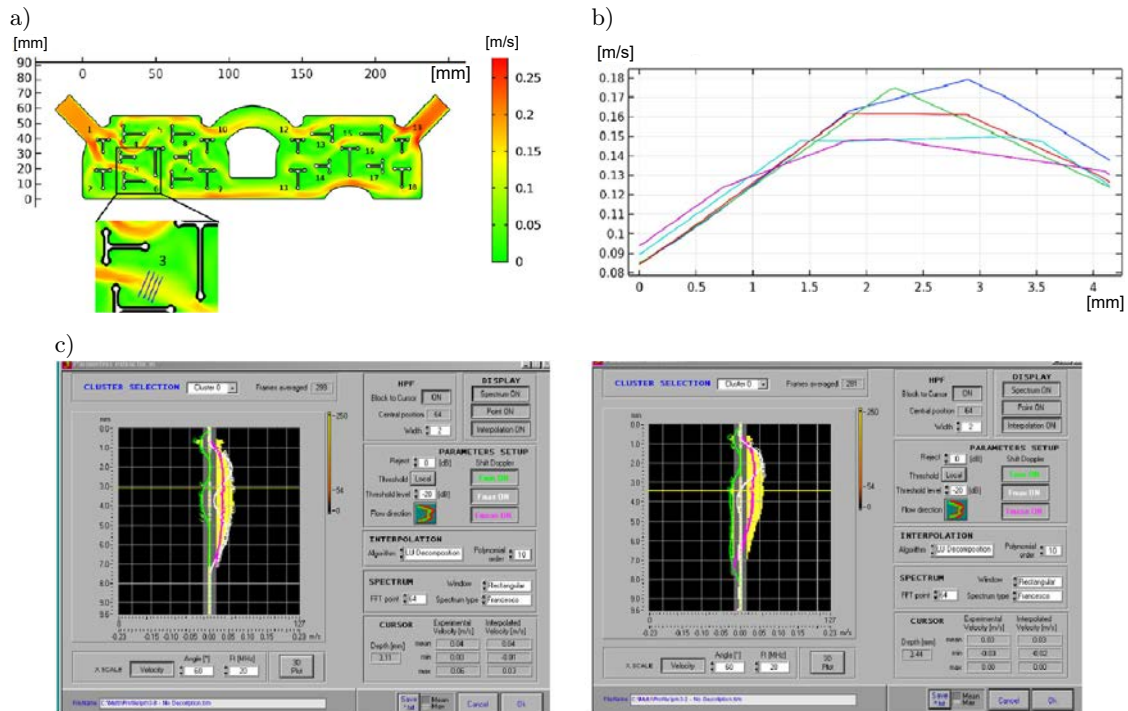


Fig. 11. Example of flow velocity profiles at point no. 3: a) location of point 3, the enlarged view shows the flow stream cross-sections for which velocity profiles were calculated numerically; b) calculated velocity profiles on these selected cross-sections; c) two examples of Doppler measurements of velocity profiles.

Table 1. Comparison of the results of experiments and numerical velocity in a fluid [cm/s].

| Point | 1 | 2 | 3 | 4 | 5 | 6 | 7 | 8 | 9 | 10 | 11 | 12 | 13 | 14 | 15 | 16 | 17 | 18 | 19 |
|---------|----|-----|------|------|------|------|-----|------|-----|-------|------|-----|------|-----|------|------|------|------|------|
| Exp. | 17 | 2.1 | 3.1 | 13.3 | 7.8 | 11.8 | 6.2 | 9.7 | 4.8 | 41.2 | 4.2 | 8.4 | 12.2 | 3 | 13.8 | 10.3 | 10.8 | 3 | 16.1 |
| Num. | 17 | 3.5 | 4.4 | 12.9 | 8.8 | 12.2 | 6.5 | 10.3 | 5.1 | 17.4 | 7.6 | 9.2 | 10.1 | 3.3 | 13.3 | 10.7 | 11.4 | 7.1 | 16 |
| % error | 0 | 40 | 29.5 | 10.8 | 11.4 | 3.3 | 4.6 | 5.8 | 5.9 | 136.8 | 44.7 | 8.7 | 20.8 | 9.1 | 3.8 | 3.7 | 5.3 | 57.7 | 0.6 |

irregular boundaries, see the USG image of KCJ surfaces in Fig. 10. The average velocities obtained by Doppler measurements near the 19 measurement points (see Table 1) were calculated by averaging 10 profiles measurements and averaging by the time variable over the complete peristaltic pump cycle. Analogously, we performed the ultrasonic measurements and MES predictions of flow velocity fields in two other prototypes: M (medium) and L (large). We did not include these results due to the qualitative similarities of the experimental and computational procedures. The differences in percent errors between the FEM predictions and the ultrasonic measurements in the M and L prototypes are slightly larger due to the larger flow space sizes in the KCJ channel system. The accuracy of the assumption of the laminar flow character in FEM modelling decreases with increasing Reynolds and Dean numbers. It should be noted that the effect of heat transport through the side walls of KCJ in the stationary temperature distribution is limited to a thin layer which is 2–3 mm thick. Inside the KCJ, the temperature nowhere rises above 12°C, even though the differences in flow velocities are even threefold, see Fig. 7.

To graphically compare the values of “global” flow velocities obtained from the measurements and the numerical model, understood here as the average of all measurement data from 19 points in the entire flow space, two boxplots, Figs 12 and 13, are shown. Figure 13 shows this comparison after excluding the outlier from the measured data set. The outlier was a measuring point no. 10 and the mean flow velocity value measured by Doppler was 41 cm/s. It was a point located on the edge of the sharp fold of the Jacket wall. The outlier measurement effect may be related to the significant curvature of the flow stream and narrowing of the flow lumen at this point resulting in the very high velocity. This situation was not reflected in the numerical calculations, the model is idealised 2D and the stream near point no. 10 has no high curvature, the Dean number in this point is of the order 1.

The difference between the global mean of the flow velocity Doppler measurements and the prediction of the numerical model is 11% of the numerical value. The numerical values of almost 60% of the results of both measurements differ significantly less than the 10% of velocity predicted by the FEM model. We emphasize that the SD of Doppler measurements is more than 10% of the mean value. Moreover, the measurements at individual points and the prediction

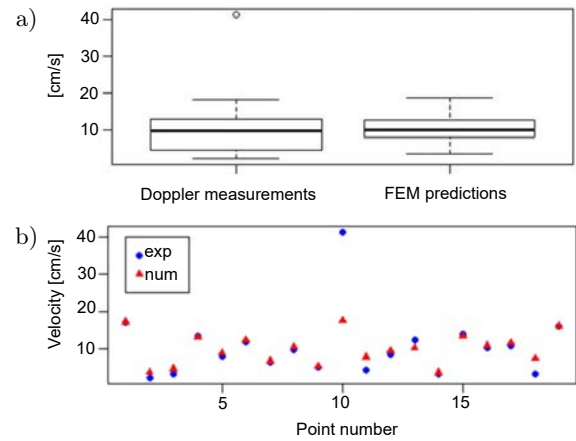


Fig. 12. a) Global velocity values from FEM model and from Doppler measurements; b) mean values of velocities in particular 19 points; the symbol “exp” in inserted legend denotes Doppler measurements and “num” depicts FEM predictions.

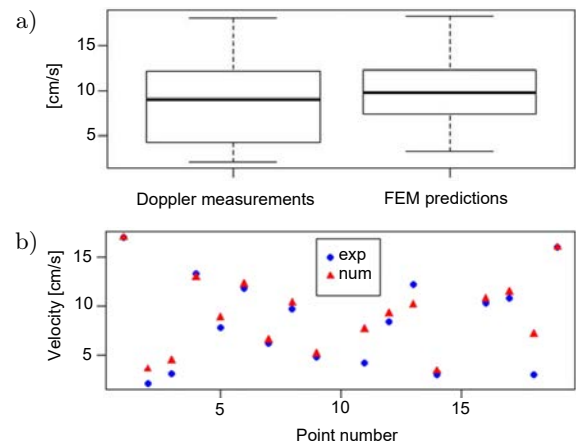


Fig. 13. a) Global velocity values from FEM model and from Doppler measurements without the outlier point no. 10; b) mean values of velocities in particular 18 points; the symbol “exp” in inserted legend denotes Doppler measurements and “num” depicts FEM predictions.

results of the FEM model are statistically strongly correlated, the Pearson correlation coefficient is 0.74 (p -value = 0.0004). Maintaining the angle, denoted by θ in Subsec. 2.3, cf. Fig. 5, between the flow direction and the beam direction, fails in places where the flow changes direction abruptly. These are such areas of KCJ where two side walls come together by folding them into a 3D shape of KCJ. The 2D model, which is the image of the projection of the structure

on the plane after “cutting” the KCJ into two halves, does not reflect in any sense the effect of the three-dimensional geometry of the flow. The measurements carried out in points no. 9, 10, 11, 13, and 18 differ more from the values obtained from the numerical model than in the other points. The sensitivity of the measurement to set the direction of the ultrasound head to the direction of flow unknown at the time of the experiment causes that the obtained velocity approximation may contain such relative errors. This was pointed out in Sec. 2 while commenting on the sensitivity of the velocity to the angle θ . The real curvature of the flow path implies complication in the measuring of an angle between flow direction and ultrasonic beam direction, which is very important in the velocity assessment by the ultrasonic Doppler measurement discussed in Subsec. 2.3. The effect of blood vessel curvature on Doppler measurements in steady flow was discussed in (BALBIS *et al.*, 2004). The relative difference between the Doppler velocity measurement and the data from the FEM model, i.e. the percentage error with which the model agrees with the measurement, is 8.8%. In addition, if we omit the values from points no. 9, 13, and 18 this error is even smaller and drops to the value of 4.6%.

Measurement integrated with ultrasound imaging of the wall structure that restricts the flow would enable identification of the stream direction and precise targeting of the ultrasound beam about the flow direction but it was not performed here. Such measurements were performed, e.g. in (NOWICKI *et al.*, 2019).

Generally, the form of the flow spaces inside KCJ side walls causes the Dean number to be very high in the places when the internal “T-letters” are located on the way of the fluid stream. But we restrict considerations to the main streams character, which is much closer to the situation when the Dean number is of the order 1, which justifies the assumption of laminar flow in the idealised FEM model.

4. Conclusions

The greatest discrepancies between the Doppler measurement of the flow field velocity and the numerical calculations appear in places where the curvature of the flow tube is not equal to zero and in the points located on the channels connecting the two parts of the KCJ which are strongly bent in space. Note that the flow space was not axially symmetrical with respect to the flow direction. Despite this, the measurements were consistent with an error less than 5% in more than 80% of measurements points. We underline that the angle between the flow direction and the beam direction was set to 60°C. Only if the measurements were made at the points where it was difficult to record a profile close to the laminar one, the velocity field values determined from the 2D model strongly

deviated from the measurements. The velocities field obtained with Doppler were sufficiently consistent with the numerical calculations, which proves that the use of a simple 2D model is precise enough to design the geometric structure of the flow ensuring the cooling homogeneity of the organ located inside the KCJ.

References

- BALBIS S., GUIOT C., ROATTA S., ARINA R., TODROS T. (2004), Assessment of the effect of vessel curvature on Doppler measurements in steady flow, *Ultrasound in Medicine and Biology*, **30**(5): 639–645, doi: 10.1016/j.ultrasmedbio.2004.02.006.
- BAMBI G. *et al.* (2004), A novel ultrasound instrument for investigation of arterial mechanics, *Ultrasonics*, **42**(1): 731–737, doi: 10.1016/j.ultras.2003.11.008.
- BREDA A. *et al.* (2022), Intracorporeal versus extracorporeal robot-assisted kidney autotransplantation: Experience of the ERUS RAKT working group, *European Urology*, **81**(2): 168–175, doi: 10.1016/j.eururo.2021.07.023.
- EVANS D.H., JENSEN J.A., NIELSEN M.B. (2011), Ultrasonic colour Doppler imaging, *Interface Focus*, **1**(4): 490–502, doi: 10.1098/rsfs.2011.0017.
- HEYLEN L., PIRENNE J., NAESENS M., JOCHMANS I. (2021), “Time is tissue” – A minireview on the importance of donor nephrectomy, donor hepatectomy, and implantation times in kidney and liver transplantation, *American Journal of Transplantation*, **21**(8): 2653–2661, doi: 10.1111/ajt.16580.
- KHAN T. *et al.* (2021), Protection from the second warm ischemic injury in kidney transplantation using an ex vivo porcine model and thermally insulating jackets, *Transplantation Proceedings*, **53**(2): 750–754, doi: 10.1016/j.transproceed.2021.01.037.
- KORCZAK-CEGIELSKA I., BREDA A., DECEWICZ A., BRODACZEWSKI K. (2022), *Kidney cooling system*, Accepted US Patent Application, No US17/666,010 (February 7, 2022).
- MOERS C., PIRENNE J., PAUL A., PLOEG R.J. (2012), Machine perfusion or cold storage in deceased-donor kidney transplantation, *The New England Journal of Medicine*, **366**(8): 770–771, doi: 10.1056/NEJMc1111038.
- NOWICKI A. *et al.* (2019), Assessment of high frequency imaging and Doppler system for the measurements of the radial artery flow-mediated dilation, *Archives of Acoustics*, **44**(4): 637–644, doi: 10.24425/aoa.2019.129276.
- SECOMSKI W., NOWICKI A., TORTOLI P., OLSZEWSKI R. (2009), Multigate Doppler measurements of ultrasonic attenuation and blood hematocrit in human arteries, *Ultrasound in Medicine and Biology*, **35**(2): 230–236, doi: 10.1016/j.ultrasmedbio.2008.08.009.